J. Electrochem. Sci. Eng. **16** (2026) 2983; *https://doi.org/10.5599/jese.2983*

Open Access : : ISSN 1847-9286
https://pub.iapchem.org/ojs/index.php/JESE

Original scientific paper

Growth of a W/TiN-bilayer coating: an alternative to diffusion barrier keeping the hard coating condition of the system

Amilkar Fragiel[1], Francisco Solis-Pomar[2,✉], Abel Fundora[3], Bernardo Campillo[4], José María Malo-Tamayo[5], Ana María Campos-Chinchilla[1], Aly Castellanos-Suárez[1], Mercedes Teresita Oropeza-Guzmán[6] and Eduardo Pérez-Tijerina[2]

[1]Centro de Física, Instituto Venezolano de Investigaciones Científicas - IVIC, Apartado 20632, Caracas 1020-A, Venezuela
[2]Universidad Autónoma de Nuevo León, Centro de Investigación en Ciencias Físico Matemáticas, Facultad de Ciencias Físico-Matemáticas, Av. Universidad S/N. Ciudad Universitaria, 66451, San Nicolás de los Garza, Nuevo León, México
[3]Instituto Superior de Tecnologías y Ciencias Aplicadas, Universidad de la Habana, Ave. Salvador Allende Nº 1110 CP 10400, La Habana, Cuba
[4]Instituto de Ciencias Físicas, Universidad Nacional Autónoma de México - UNAM, Av. Universidad s/n, Col. Chamilpa, Cuernavaca, Morelos, México
[5]Instituto Nacional de Electricidad y Energías Limpias, Av. Reforma 113, Col. Palmira, Cuernavaca 624490, Morelos, México
[6]Tecnología Nacional de México, Instituto Tecnológico de Tijuana, Departamento de Ingeniería Química y Bioquímica, Calzada Tecnológico s/n, Fraccionamiento Tomas de Aquino, Tijuana, Baja California, México

Corresponding Author: ✉francisco.solispm@uanl.edu.mx; Tel.: +52 8183294000

Received: September 9, 2025; Accepted: December 21, 2025; Published: January 2, 2026

Abstract

An evaluation of the improvement provided by a W thin film, when incorporated into a TiN bilayer coating system on 304 stainless steel, is reported after determining its electrochemical behaviour and mechanical properties. The TiN-bilayer and W/TiN-bilayer coatings were prepared by balanced magnetron sputtering. Coating structure, morphology, interphase, and chemical composition were determined by scanning electron microscopy, Auger electron spectroscopy and X-ray diffraction. Mechanical properties were determined by the nanoindentation technique. The electrochemical behavior was investigated by electrochemical impedance spectroscopy (EIS) using 6 wt.% NaCl solution as electrolyte. The electrochemical results showed an increase in overall corrosion resistance (R_p) when the W thin film is incorporated into the TiN-bilayer coating system. The R_p for the initial measurement is 187.6 and 347.9 kΩ cm^2 for the TiN-bilayer coating system and W/TiN-bilayer coating system, respectively. The results obtained from the EIS study over time indicate that the R_p after 7 weeks of immersion *are 53.2 and 119.8 kΩ cm^2 for the TiN-bilayer coating system and W/TiN-bilayer coating system, respectively. Nanoindentation hardness measurements showed a slight difference between the two coating systems. The TiN-bilayer hardness showed a value of approximately 24 GPa, while the W/TiN-bilayer hardness showed a value of approximately 22 GPa. Considering other beneficial properties associated with W, the results showed that a W/TiN-bilayer coating system can be used as an alternative hard and protective coating system on steel substrates to mitigate corrosion damage.*

Keywords
Two-layer coatings; tungsten thin films; magnetron sputtering, nodular defects, diffusion barrier

Introduction

Tungsten (W) is a refractory metal with high wear resistance and a low coefficient of friction, high hardness, and high resistance to corrosion and oxidation. Because of these properties, W thin films have been used for a variety of applications [1]. W compounds, such as WC, have also been successfully used as hard-coatings [2]. This element has also been studied for other properties such as low hydrogen permeability, high thermal conductivity, and the lack of chemical reaction with hydrogen, properties that make it a candidate plasma coating material for fusion reactors [3]. Physical vapor deposition (PVD) methods, such as magnetron sputtering (in RF or DC mode) and high-power pulse magnetron sputtering, are commonly used to deposit W [4]. Ar gas pressure, substrate temperature, substrate material, and deposition rate are among the parameters that define the presence and relative amounts of the β-W and/or α-W phases [5]. In W films obtained by a sputtering process, α-W may be in an equilibrium state, but β-W is usually present in a meta state, or the film may be formed as a mixture of two phases [6]. In previous work, Fritze *et al.* found that carbon addition has a grain-refining effect on W films. In addition, Fritze et al. also found a hardness value of about 13 GPa for pure W thin films obtained by a sputtering process using a single crystal of α-Al_2O_3 as a substrate [7].

On the other hand, metal nitrides are well known for their excellent wear and corrosion resistance and high melting points, which make them attractive for hard-coating applications in the tool and decorative industries [8]. In particular, titanium nitride (TiN) has been extensively studied for certain applications [9]. For example, Yang *et al.* [10] synthesized Cu nanoparticles by electrodeposition on TiN-coated electrodes. They found that pyramidal TiN morphologies yield irregular Cu nanoparticles, whereas granular TiN films yield octahedral Cu nanoparticles [10]. In addition, TiN coating has been used to improve the corrosion resistance of bipolar plates in fuel cells [11]. In fact, TiN is emerging as an attractive coating material for damping mitigation due to its high hardness, chemical stability, and low electrical resistivity [12]. Furthermore, the aerospace industry´s requirements for high strength and good corrosion resistance, among others, have made titanium coatings an excellent choice over steel and aluminum [12]. The biomedical industry has also shown interest in TiN coatings, mainly due to their excellent biocompatibility. Titanium-based coated materials have potential applications as buffer layers that serve as a “bond” between coatings, such as amorphous carbon on stainless steel [13]. In addition, Subramanian et al, found that TiN has good hemocompatibility when the Ni film is used as a buffer between stainless steel and the TiN coating [14]. Thus, considering the various applications of TiN coatings and the properties of W and TiN (coating roughness, hardness, corrosion and abrasion wear resistance) [15], the

W/TiN system could be an interesting hard coating alternative for diffusion barriers and high temperature stability.

In this study, TiN-bilayer and W/TiN-bilayer coatings systems were prepared by reactive balanced magnetron sputtering using a 304 stainless steel (304SS) as a substrate in order to compare the mechanical properties and electrochemical behaviour of the two types of coating systems and to determine the influence of the W thin film when deposited on a TiN-bilayer coating. The results and implications of this work are presented and discussed in this paper.

Experimental

W/TiN-bilayer and TiN-bilayer coating systems were prepared separately by DC-balanced magnetron sputtering on 1-inch-diameter, 7-mm-thick 304 stainless steel substrate discs with a roughness (R_a) of 4.16 nm. W and, Ti commercial discs (99.9 % purity) were used as targets. The sputtering vacuum chamber was evacuated to 0.06 mPa (6.0×10^{-7} mbar) using mechanical and turbomolecular pumps. The TiN coatings were prepared at an N_2 partial pressure of 0.04 Pa and a working pressure of 0.3 Pa. The W thin film was deposited using Ar as a carrier gas at a working pressure of 0.4 Pa, with the substrate at a temperature of about 400 °C. All layers and film involved in this investigation were deposited at 200 Watts. Prior to deposition, the 304 stainless steel substrates were polished with alumina slurry to 0.3 µm, and ultrasonically cleaned in acetone and alcohol for 30 min. The substrate temperature for the TiN compound deposition was 250 °C. To obtain the TiN bilayer on 304SS (TiN bilayer/304SS), the process is defined as Process 1 (Figure 1A), and is summarized as follows: the 304SS substrate is heated to 250 °C and held at this temperature during growth of the TiN L1 and L2 layers To obtain the W thin film on the TiN bilayer/304SS substrate, the procedure is defined as process 2 (Figure 1B) and is summarized as follows: The temperature of the TiN bilayer/304SS substrate is increased to 400 °C and maintained throughout the growth of the W thin film.

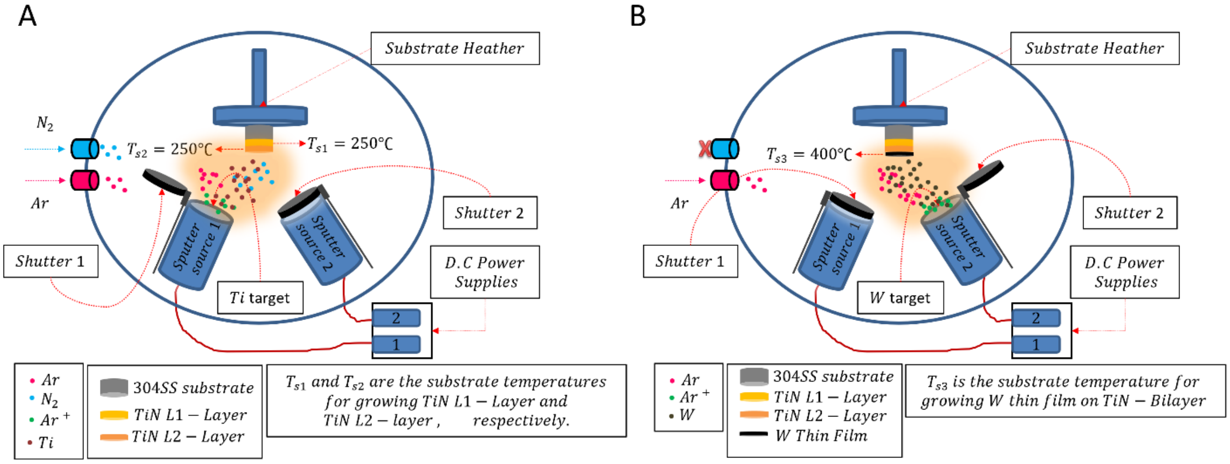

Figure 1. *A) Scheme of process 1: growth of TiN-bilayer on 304SS; B) scheme of process 2: growth of W thin film on TiN-bilayer/304SS*

Thus, process 1 is required for the production of TiN bilayer coating systems, and processes 1 and 2 are required for the production of W/TiN bilayer coating systems. The atomic concentration profile was determined by Auger electron spectroscopy (AES) using a SAM-PHI 595 instrument. The X-ray diffraction pattern was obtained using a Philips X-pert instrument with Cu Kα radiation. The morphology characteristics were obtained by scanning electron microscopy (SEM) using Jeol JSM-5300 equipment.

Mechanical properties were determined by nanoindentation tests on the coatings using a Hysitron Ubi1 instrument. The load was varied from 120 µN to 9000 µN using a pyramidal Berkovich tip on each coating system. The first measurement was made under an applied load of 120 µN and then an increase of 370 µN was made for each measurement until 9000 µN was reached. Figure 2 shows the nanoindentation process scheme.

The electrochemical behaviour of the coating systems was evaluated using electrochemical impedance spectroscopy (EIS) at the open-circuit potential (OCP). The test was performed in a three-electrode cell, where the sample was connected as the working electrode. The graphite bar and saturated calomel were used as the counter and reference electrodes, respectively. 6 wt.% NaCl solution was used as the electrolyte. The exposed area was 1 cm^2. The initial measurement was performed after 5 hours of immersion, using a sinusoidal amplitude of 10 mV over the frequency range 30000 to 0.1 Hz. For EIS over time study, measurements were made every week for seven weeks, with a sinusoidal amplitude of 10 mV applied in a frequency range of 30000 to 0.01 Hz.

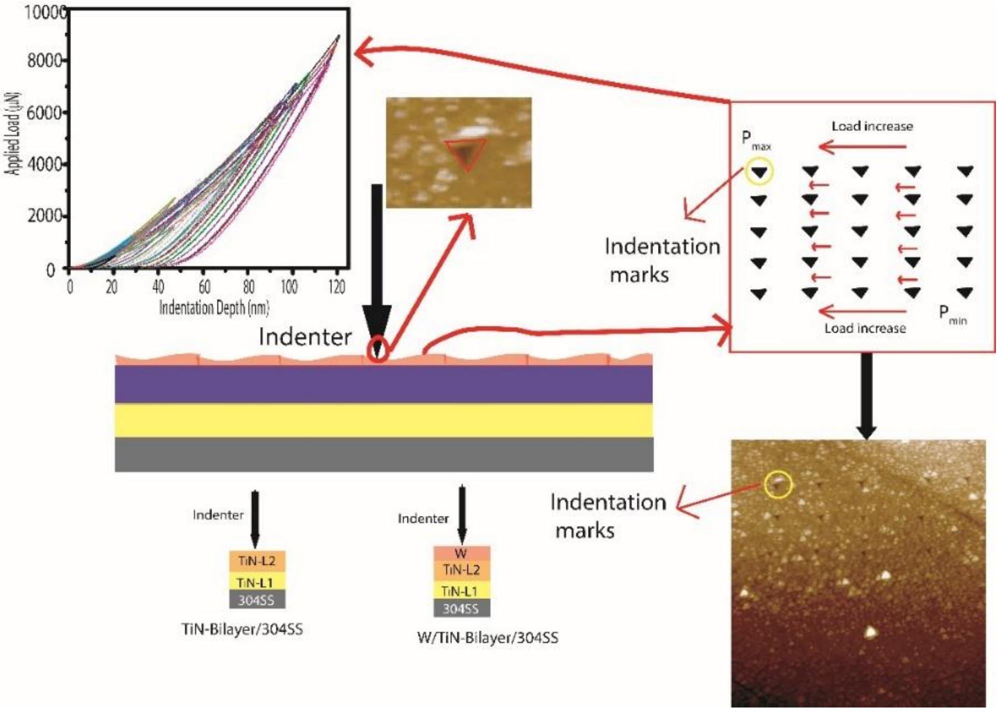

Figure 2. *Indentation process scheme*

Results and discussion

Structural characteristics of obtained coating systems

The thicknesses of the coatings deposited on the 304SS substrate were determined from scanning electron microscope (SEM) observations of the cross-section, as shown in Figures 3 and 4. Figure 3A illustrates the W/TiN-bilayer coating system. In this figure, a thin film of tungsten (W) is first observed at the surface, followed by a TiN bilayer coating and, subsequently, the 304SS substrate at the bottom. The TiN bilayer coating system comprises two layers, L1 and L2. The thickness of L1 was approximately between 3 and 4 µm in all prepared coatings, and the thickness of L2 was approximately between 1.5 and 2 µm, as shown in Figures 3 and 4. The thickness of the W thin film was approximately 160 nm.

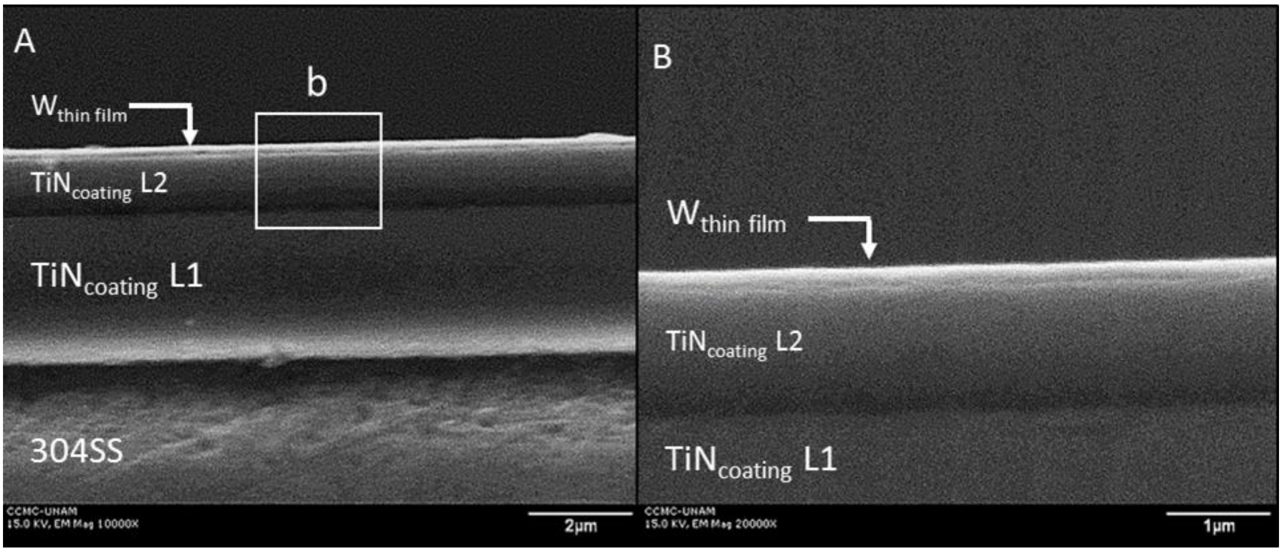

Figure 3. *SEM micrographs showing: A) cross section of W/TiN-bilayer/304SS system, B) detail b from A)*

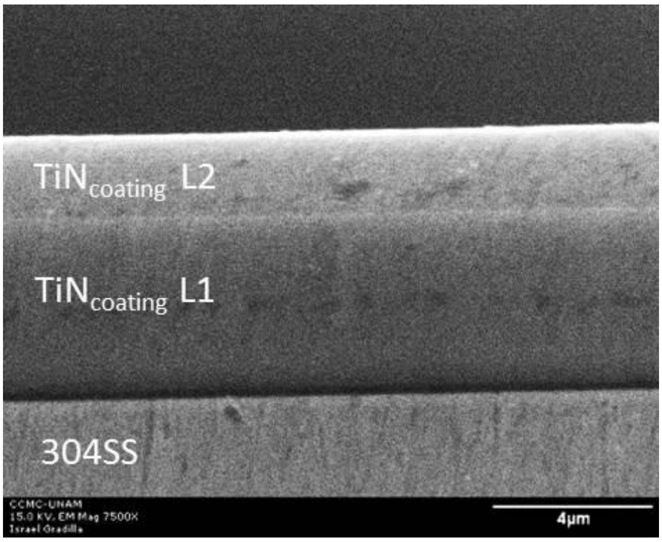

Figure 4. *SEM micrograph showing the cross-section of the TiN-bilayer/304SS system*

The X-ray diffraction pattern of the W/TiN bilayer coating system is shown in Figure 5. The W thin film grows preferentially along the [110] direction (where the highest-intensity peak is located), as reported by Sun *et al.* [16].

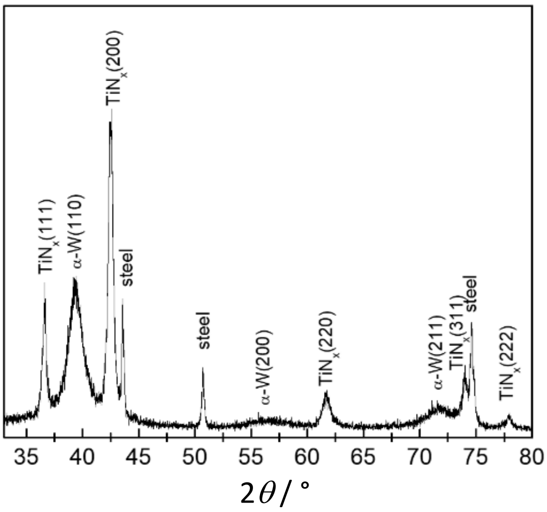

Figure 5. *X-ray diffraction pattern for W/TiN-bilayer coating system*

The peaks related to tungsten (W) in the X-ray diffraction pattern indicate the presence of the α-W phase in the tungsten film. Other preferential growth directions for W thin films have been reported by different authors, but in these cases, the substrates were silicon-related [5,17]. It is well known that the morphology and structure of thin films depend strongly on the substrate material and the initial crystal orientation [5]. In this case, the W film grew in the [110] direction on a TiN substrate (layer L2). For the TiN compound, the preferred growth direction was [200] (the highest-intensity peak), but the XRD pattern also shows growth in other directions, such as [111], [222], [220] and [311], which have been reported elsewhere [18].

The composition of the W/TiN coating system was confirmed by the AES depth profile (Figure 6) for the W thin film and TiN layer. The AES analysis results revealed the presence of a small amount of carbon in the coating system. It should be noted that the presence of carbon and oxygen in the film may be due to residual gases, such as methane and carbon dioxide, in the vacuum chamber at pressures approaching 0.01 mPa. Additionally, previous work has shown the presence of CN molecules in the plasma using optical emission spectra, which is related to the presence of carbon in the chamber [19]. On the other hand, AES results clearly demonstrate a diffusion zone in which W diffuses towards the L1 layer and TiN diffuses towards the W thin film. Therefore, it can be concluded that the W-TiN composite is part of the W thin film and also forms an interface with the L2 layer. In fact, the profile shows that, at a certain distance from the surface, the lines corresponding to W and Ti intersect at a point (see Figure 6A for detail) where the atomic concentration is about 48 %.

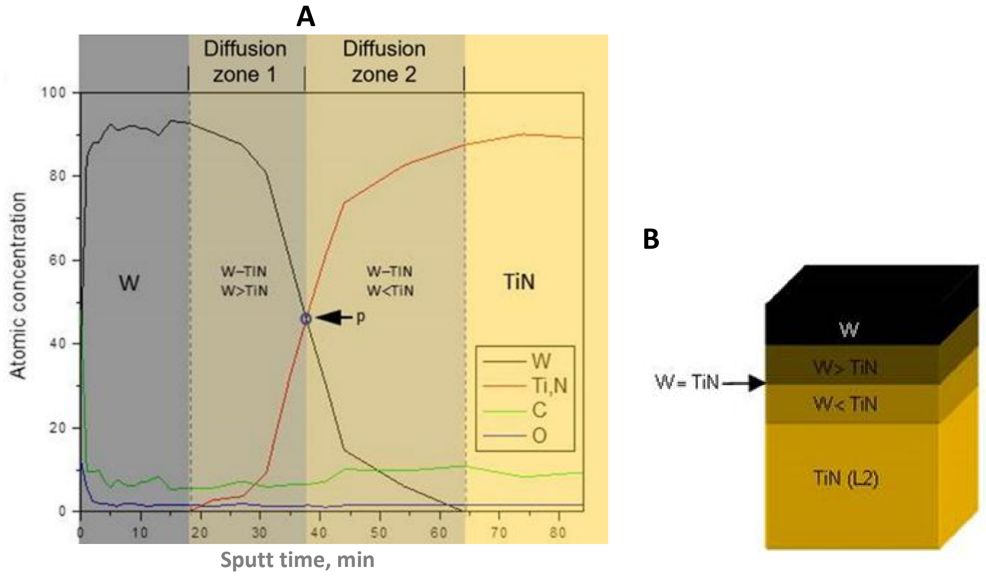

Figure 6. *A) Auger depth profile for W/TiN-bilayer coating system; B) schematic representation of the W thin film and diffusion zone formed between the W film and the L2 layer*

This could indicate the interface between the W film and layer L2. From this point to the left is the diffusion zone (see diffusion zone 1 in Figure 6), which affects the W thin film directly, and to the right is the diffusion zone (see diffusion zone 2 in Figure 6), which affects the L2 layer. In either case, the W-TiN composite forms on both sides, and the two diffusion zones together form a strong interface that could contribute significantly to the properties of the W/TiN-Bilayer coating system, such as its mechanical and corrosion properties. Previous work has shown that the diffusion of W, Ti and N can be achieved by annealing W-Ti-N films after sputtering in a vacuum chamber [20]. In our case, we believe that the diffusion process was activated during sputtering, given that the deposition temperature of the W film was 400 °C. This temperature can promote diffusion on the substrate surface (layer L2) and diffusion of elements between layers (layer L2 and the W film). The mixture between TiN and α-W in the W-Ti-N films has been reported elsewhere [21].

Both the L1 and L2 TiN layers have a pyramidal grain structure (see Figure 7A). The presence of pyramidal grains could be mainly due to the substrate temperature (T_s), because it is well known that at low temperatures relative to the melting point (T_m) of the condensed material, pyramidal grains tend to be formed [22]. In fact, this type of structure is categorized by the Thornton model as a Zone 1 structure and tends to form when the T_s/T_m ratio is between 0.1 and 0.3. In this case, we found that the pyramidal grain structure appeared below this range, specifically between 0.06 and 0.1. However, the cause is the same: a T_s value that provides a T_s/T_m ratio of 0.3 or less. On the other hand, in crystallographic terms, the presence of a pyramidal grain structure can be attributed to the [111] preferred orientation, while the columnar structure is favoured by the [200] preferred orientation [23]. However, in this investigation, the X-ray diffraction results for the pyramidal grain structure indicate that the highest-intensity peak corresponds to the [200] orientation, with the [111] orientation contributing a minor peak. Taking into account that the global energy of a film or coating comprises strain energy and surface energy, with the [111] orientation having the lowest strain energy and the [200] orientation having the lowest surface energy, as well as the fact that variations in crystallographic orientations are mainly caused by competition between surface energy and strain energy [24], It is therefore possible to suggest that the TiN pyramidal structure obtained in this research may be associated with a transition from the [111] orientation to the [200] orientation due to the competitive effect of strain and surface energies. Although the [111] orientation has a lower intensity peak than the [200] orientation, the pyramidal grain structure still prevails. In general terms, the crystallographic orientations are strongly influenced by adatom mobility, surface energy, strain energy and diffusivity energy, factors which in turn are very influenced by deposition parameters [24], and therefore, in the case of this investigation, the substrate temperature is a key parameter during the growth of the TiN pyramidal grain structure.

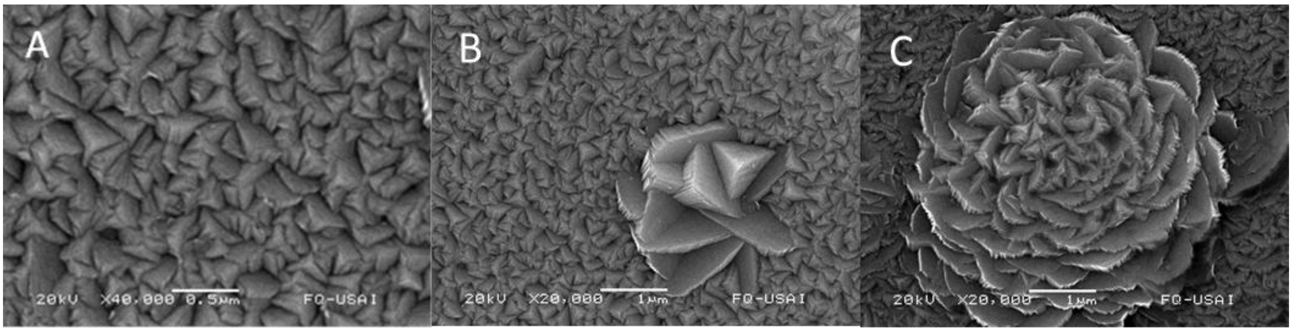

Figure 7. *SEM micrographs showing: A) the grain structure obtained at the layers L1 and L2; B) and C) several defects found in TiN coatings on 304SS at 180 °C*

It is important to note that, prior to preparing both coating systems for this investigation, TiN coatings were deposited on a 304SS substrate at 180 °C. A significant number of nodular defects were observed, and their structure is shown in Figure 7B. These defects are generally initiated by a seed, which is usually related to dust, impurities, and droplets (macroparticles) trapped in the coating. These particles can also originate from the target during the sputtering process, or from the vacuum chamber components [25]. These seeds produce an abnormal growth with respect to the growth of the film, usually forming a defect with a semicircular cap shape [26]. Indeed, the nodular defect structure shown in Figure 7B suggests abnormal pyramidal grain growth.

It is important to note that, in our work, we have observed that defect growth can be complex in some cases because defects can reach large sizes and take particular shapes. An example of such situations is shown in Figure 7C, where a large size and a rose shape are seen. This type of defect was observed only in the L1 layer, corresponding to the TiN compound deposited directly on 304SS. Therefore, these nodular defects may be directly related to the steel surface, as cracks, a very rough surface, scratches, inclusions and impurities act as preferential nucleation sites, resulting in isolated and complex nodular-type overgrowth structures [27].

As discussed in previous paragraphs, the substrate temperature is a key deposition parameter because higher temperatures can enhance surface diffusion in the PVD process. This can be beneficial in reducing physical defects, but it may introduce the risk of chemical activity, as discussed elsewhere [28]. In our case, increasing the substrate temperature to 250 °C drastically reduced the presence of overgrowth defects in the L1 layer, resulting in fewer defects and a significant reduction in their size. Therefore, the TiN layers involved in both systems were deposited at a substrate temperature of 250 °C. This suggests that substrate temperature is an important factor in mitigating anomalies in layers prepared by magnetron sputtering. Figure 8A shows that the W thin film has nodular defects (red arrows) and possible pinholes (green arrows) on its surface, indicating that defect formation may be inherent in the growth of coatings and films by the magnetron sputtered process, regardless of the deposited compound. In coatings, the presence of defects is critical because they can provide pathways for electrolyte diffusion to the substrate surface. Large defects, in particular, can create microporosities that act as diffusion pathways for ions that promote corrosion of the substrate [29].

Figures 8A and 8B show the cracks formed in the L1 layer. These cracks were only observed in some specimens and were always present in the L1 layer. Although cracks can usually also form inside the layer due to defects and particles on the steel surfaces, we believe that the presence of cracks in the L1 layer is more likely to be related to expansion problems, primarily due to the temperature at which the W thin film was deposited (400 °C), since these cracks were mainly found in the L1 layer involved in W/TiN-bilayer coating system.

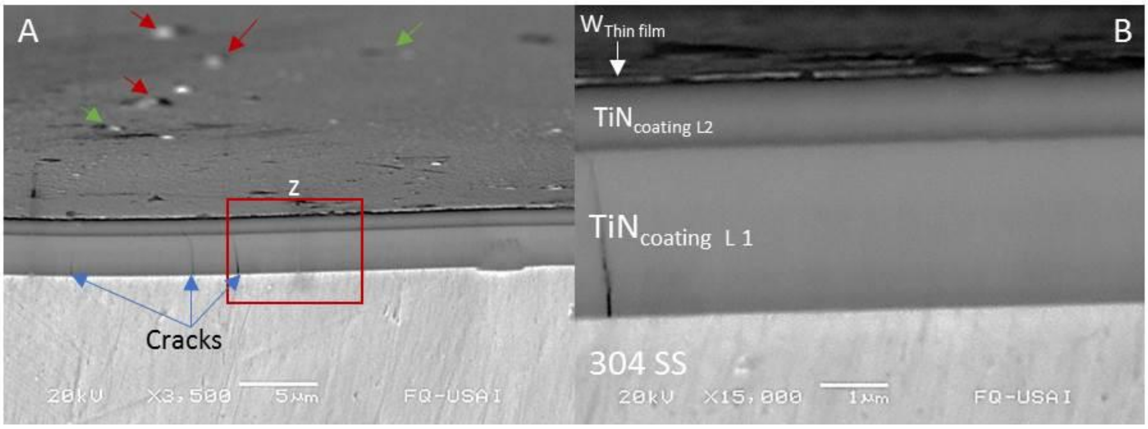

Figure 8. *A) SEM micrographs that show cracks present in the layer L1 of the W/TiN-bilayer coating system, pinholes and nodular defects in the W thin film; B) detail z from A)*

It is also important to note that the irregularities present in the substrate surface, such as slope zones, can cause defects and some zones with a lack of adhesion in the substrate-coating interface (Figure 9). In addition, sputtered coatings tend to reflect the substrate surface almost exactly; this feature is evident in Figure 9, where the substrate's slope zone is clearly reflected in the coating. Therefore, it is very important that the preparation and cleaning of the substrate prior to the sputtering process are extremely careful to avoid defects, cracks, poor adhesion zones in the substrate-coating interface and thus obtain layers that could be free of these problems to a certain extent.

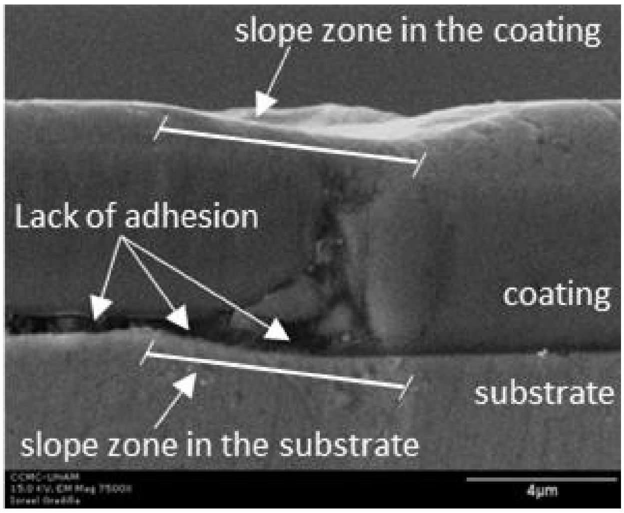

Figure 9. *Slope zones on the surface of the substrate may promote a lack of adhesion and defects*

Electrochemical behaviour

In this study, electrochemical impedance spectroscopy (EIS) was used to investigate corrosion phenomena in coating systems produced by sputtering. However, it is important to note before starting the analysis that the data provided by the EIS technique are closely related to dielectric behaviour, oxidation-reduction reactions, and mass migration, all of which are determined by the chemical and electrical properties of the corrosion medium and the materials [30]. Impedance (Z) can be expressed as a complex number, where the real component is associated with resistance, while the imaginary component represents capacitance and/or inductance. All the obtained data can be displayed in Nyquist plots ($-\underline{Z}_{\text{imag}}$ *vs.* Z_{real}) and Bode plots (log impedance modulus and phase angle vs. log frequency). The EIS data can be fitted using equivalent circuits (ECs), in which each part of the system is represented by an electronic circuit based on a specific impedance combination.

The first approach in studying the corrosion properties of the system using EIS is to compare the diameters of the semicircles in the Nyquist plot. Large diameters are directly related to high corrosion resistance. As an initial part of this study, the two coating systems TiN-bilayer/304SS and W/TiN-bilayer/304SS were evaluated after five hours of immersion in 6 wt.% NaCl solution, and in addition, the uncoated 304 SS was also evaluated for comparison purposes. The semicircles in the Nyquist plot (Figure 10A) corresponding to the initial measurement of two coating systems and uncoated 304 SS, reveal that the W film incorporated into the TiN-bilayer coating system contributes significantly to corrosion resistance. In this case, the W film on the TiN-bilayer coating system has a larger diameter than the TiN-bilayer coating system. These results indicate an improvement in the corrosion resistance of the coating system containing W. Furthermore, they reveal that both coating systems (W/TiN-bilayer and TiN-bilayer) exhibit superior corrosion resistance compared with uncoated 304 SS.

Figure 10B shows the Bode plot (phase angle (θ) *versus* log frequency (f)) for the initial measurement. The θ) response for both coating systems shows a broad peak in the high-frequency range, which is close to -90°, indicating capacitive behaviour, which is a typical response of a good coating. A high θ (close to -90°) indicates a very low level of heterogeneity at the surface, which is directly related to greater corrosion resistance. In fact, when the θ is -90°, the coating behaves like an ideal capacitor, implying dielectric behaviour of the coating. When the θ is 0°, the coating behaves like a resistor [31]. Therefore, the peaks located in the high-frequency range are related to the coating and its defects. Conversely, the peaks located in the low-frequency range are related to the corrosion process at the substrate-coating interface. However, in EIS studies of coatings, processes in both the high- and low-frequency ranges are closely related. This makes it possible to observe the response of defects and cracks in the coatings at the substrate-coating interface. Figure 10B shows that the peak associated with the W/TiN-bilayer system lies above that of the TiN-bilayer system, indicating a smaller angle (closer to -90 °). This suggests that the W thin film enhances the corrosion protection of the TiN-bilayer system. Figure 10C presents the Bode plots (log impedance modulus (|*Z*|) *vs.* log frequency (*f*)), showing the smallest impedance for the uncoated 304 SS and the highest for W/TiN-bilayer at almost all frequencies.

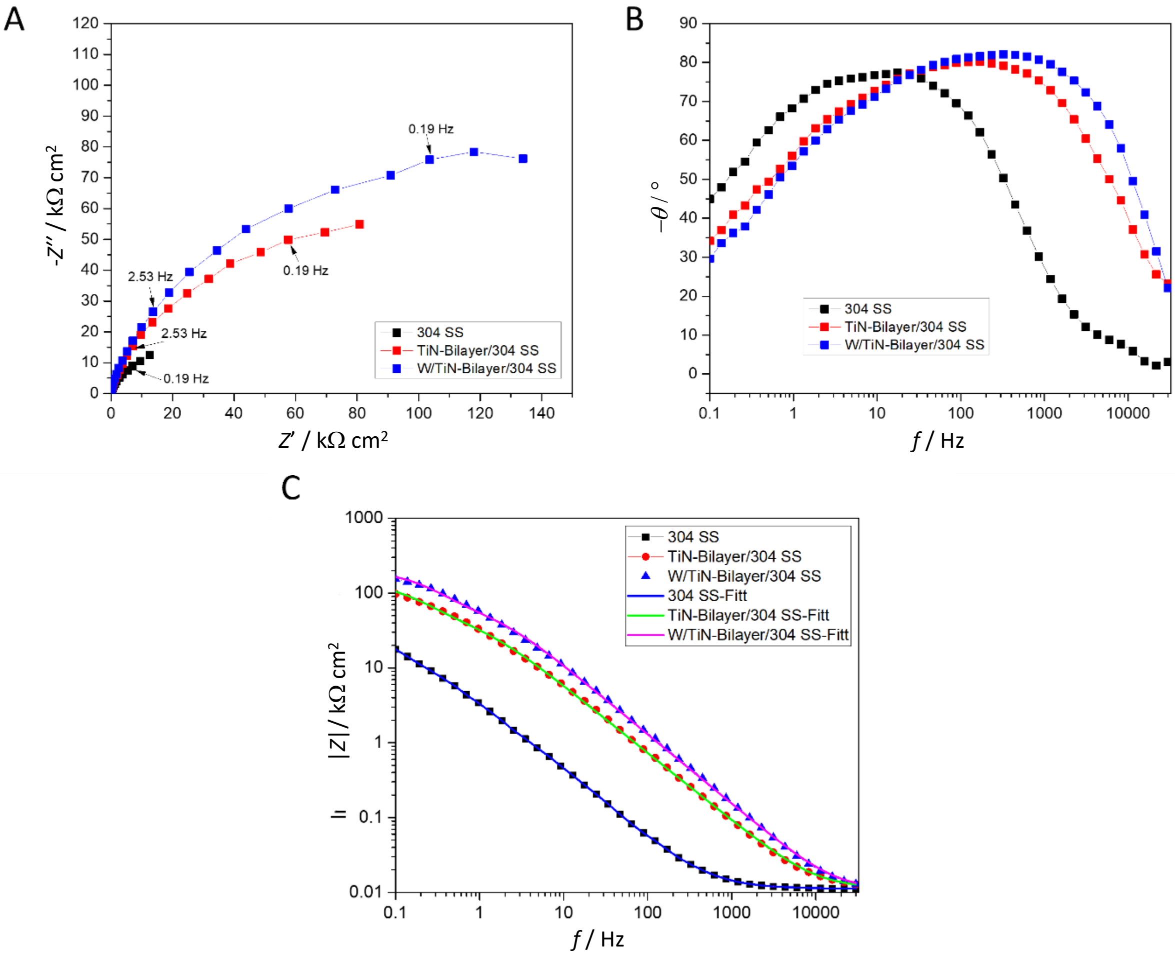

Figure 10. *EIS plots for uncoated 304 SS, TiN-bilayer/304 SS and W/TiN-bilayer/304 SS taken after five hours of immersion in a 6 wt.% NaCl solution; A) Nyquist plots and Bode plots B)* θ vs. *log* f *and C) log|Z|* vs. *log* f. *Presented fitting results are obtained using the corresponding equivalent circuits*

To better understand the EIS data of the systems under study, equivalent circuits (ECs) were employed. Figure 11 shows the ECs used to fit the EIS data.

The ECA was used to fit the EIS data of the coating systems. This EC has previously been used for coatings [32]. The EIS data for uncoated 304SS were fitted using the ECB, which has also been used elsewhere for uncoated stainless steel [33]. It is important to note that the pure capacitor is replaced by a constant phase element (CPE) in the EC fittings, because the CPE accounts for surface heterogeneities. The CPE is commonly used in previous works and its impedance, Z_{CPE}, is defined by Equation (1) [34]:

$$Z_{\mathrm{CPE}} = Q^{-1} (j\omega)^{-n} \qquad (1)$$

where Q is the quasi-capacitive parameter, ω is the angular frequency, and j is the imaginary unit. The n parameter is the CPE exponent, which lies between 0 and 1. As n approaches 1, the CPE response approaches the ideal behaviour of a homogeneous capacitor, whereas as n approaches 0, the response approaches resistive behaviour [35].

In both ECs shown in Figure 11, R_{sol}, Q_{dl} and R_{ct} represent solution resistance, double layer capacitance and charge-transfer resistance, respectively. For the ECA, other electronic components were used to represent the coating. These components are the coating capacitance Q_{c}, and the coating resistance R_{c}. R_{c} refers explicitly to the pores or channels through which the aggressive medium penetrates towards the substrate. Throughout this paper, we will refer to these pores or channels as pathways.

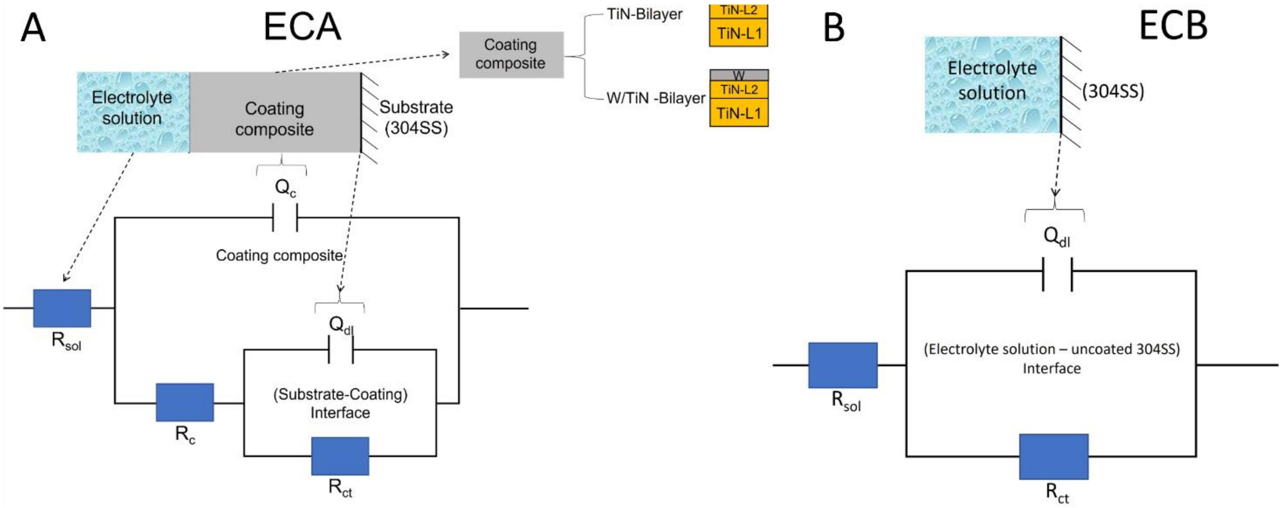

Figure 11. *A) Equivalent circuit (ECA) used for TiN-bilayer and W/TiN bilayer coating systems and B) equivalent circuit (ECB) used for uncoated SS 304*

Table 1 presents the values of the electronic components used in the fitting of the initial measurements. For all fittings made in this work, the chi-squared (χ^2) is about 10^{-3} with an error per element less than 3 %.

Table 1. *EIS data obtained by fitting ECs to measured impedance spectra*

Element	304SS	TiN-bilayer/304SS	W/TiN-bilayer/304SS
R_{sol} / kΩ cm^2	0.0113	0.0114	0.011
$Q_{\text{dl}}\times10^6$ / Ω^{-1} cm^{-2} s^n	570	8.29	4.19
n_{dl}	0.86	0.60	0.61
R_{ct} / kΩ cm^2	24.729	156.002	302.990
R$_{\text{c}}$ / kΩ cm^2	-	31.617	45
$Q_{\text{c}}\times10^6$ / Ω^{-1} cm^{-2} s^n	-	3.69	1.76
n_{c}	-	0.91	0.95
R_{p} / kΩ cm^2	24.729	187.619	347.990

The results shown in Table 1, clearly confirm that the W film acts as a barrier. This barrier effectively improves the corrosion resistance of the TiN-bilayer coating system. For example, for the substrate-coating interface, the Q_{dl} decrease as follows: $Q_{\text{dl 304SS}} > Q_{\text{dl TiN-bilaver/304SS}} > Q_{\text{dl W/TiN-bilaver/304SS}}$. Accordingly, the R_{ct} increase as follows: $R_{\text{ct 304SS}} < R_{\text{ct TiN-bilaver/304SS}} < R_{\text{ct W/TiN-bilaver/304SS}}$. These results clearly show that the substrate is more effectively isolated from the electrolyte solutions by the W/TiN bilayer coating system. In the case of the coating behaviour, the Q_{c} for the W/TiN-bilayer coating system decreases with respect to the TiN-bilayer coating, and the R_{c} for the W/TiN-bilayer coating increases with respect to the TiN-bilayer coating; together with the R_p, these indicate the effective contribution of the W film to the corrosion resistance of the TiN coating system. It is also important to note that the overall corrosion resistance of the system R_p can be estimated by the sum of the resistances involved in the circuit model (R_{ct} + R_c) [36].

Moreover, the n_c obtained for the W/TiN-bilayer coating is higher than the n_c value for the TiN-bilayer. This suggests that the W film improves the coating by reducing surface heterogeneity, despite the presence of pinholes and nodular defects, as shown in Figure 8A. It is important to note that when the surface is less heterogeneous, the current flow can be distributed over the surface of the coating, thereby eliminating the concentration of current in defects such as cracks, pores and nodular defects, and thus mitigating galvanic attack [37], which is another reason why the W film improves the corrosion resistance of the coating system.

Time changes of EIS-generated coating resistances

The initial measurement (measurement after five hours of immersion) is very important because it can be used to predict how the system will perform over time. This is because the first measurement provides a snapshot of the system (in this case, the coating systems) in all its capacities.

From this point of view, and with the aim of confirming the electrochemical behavior obtained from the initial measurements of the two coating systems, an electrochemical study was carried out over time, analysing the variations in R_{ct}, R_c and R_p values. It is necessary to highlight that during each EIS measurement, the system must remain in a steady state; in fact, the low-frequency finds its limit at the stationarity [38]. Therefore, low-frequency ranges should be used rationally.

It is important to emphasize that R_{ct} is a parameter that characterises the interface (substrate-coating) and indicates the level of protection that the coating system provides against the aggressive environment to some extent. Figure 12A shows the variation of R_{ct}, R_c and R_p over time for the TiN-bilayer coating. The values of R_{ct}, R_c and R_p for weeks 1 to 5 were obtained by using ECA. The results show that R_{ct} remains almost constant during the first two weeks. However, the R_p increases during the first week compared to the initial measurements. This increase in R_p is due to a significant increase in R_c, as the coating system may experience clogging of some pathways. This partially blocks the diffusion of ions to the substrate surface or interface (substrate-coating). However, the interface may remain active if pathway clogging is insufficient to suppress electrochemical activity. Therefore, an increase in R_c does not necessarily imply an increase in the R_{ct} parameter, as the corrosion process at the substrate surface depends on coating conditions and the available pathways for the electrolyte solution to penetrate the substrate. Thus, in some cases, an increase in R_c may keep the corrosion process on the substrate surface almost unchanged (R_{ct} remains almost constant), while in others, it mitigates the corrosion process (R_{ct} increases).

In addition, when R_c remains constant over time, R_{ct} may decrease, as illustrated in Figure 12A between weeks 2 and 3. This behaviour may be due to the constant flow of ions through the pathways over time, which feeds the corrosion process and increases electrochemical activity at the substrate-coating interface (R_{ct} decreases). It should also be noted that ions diffusing towards the substrate-coating interface can promote galvanic and crevice corrosion between the coating and substrate [39], in which case the coating acts as a cathode and increases damage to the substrate surface.

Between weeks 3 and 7, the R_p remain below 80 kΩcm², where increases in R_c lead to increases in R_{ct}, while decreases in R_c favour corrosion of the substrate surface (R_{ct} decreases). However, EIS measurements taken at weeks 6 and 7 reveal unusual behaviour in the low-frequency range, as illustrated in Figures 13A to 13C.

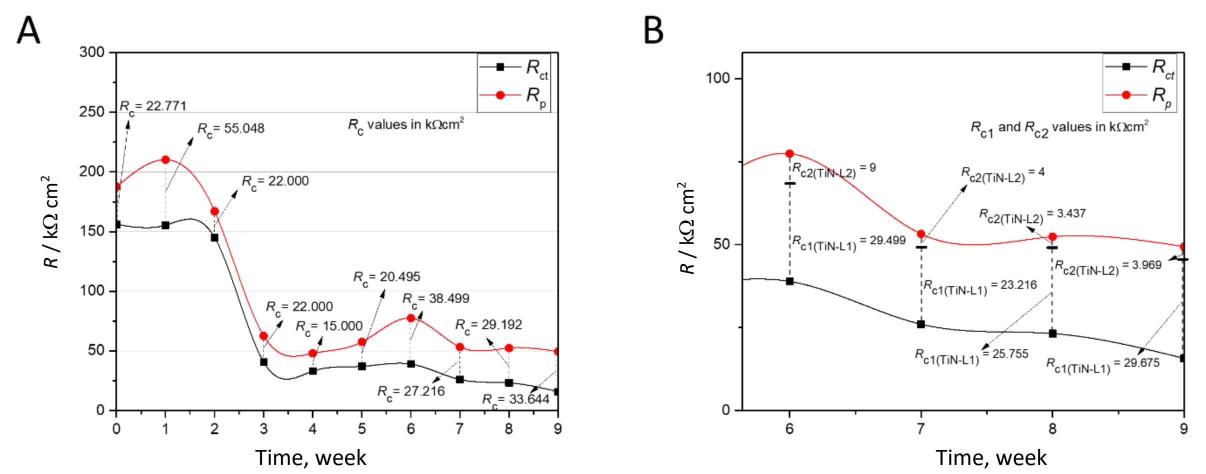

***Figure 12.** A) Time changes of EIS generated resistance values for TiN-bilayer coating; B) individual contributions of the layers L1 and L2 for weeks 6,7,8 and 9*

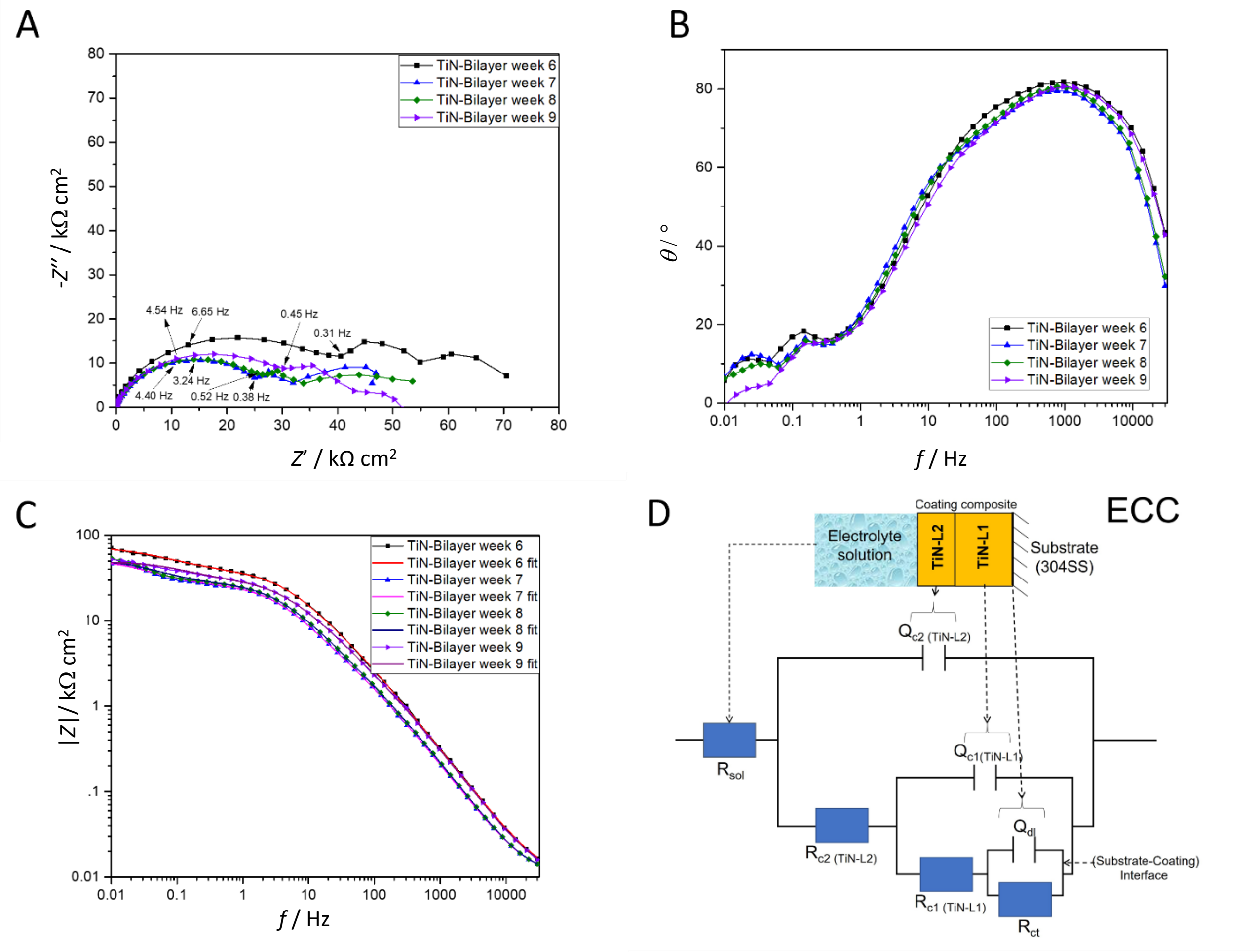

***Figure 13.** EIS plots of TiN-bilayer coating for weeks 6,7,8 and 9: A) Nyquist plots and Bode plots, B) ϑ vs. log f, C) log |Z| vs. log f; D) equivalent circuit used for fittings*

These low-frequency features may reveal the contribution of another component of the coating system to the corrosion process. In this case, the EIS technique may detect the individual contributions of the two TiN layers involved in the TiN-Bilayer coating system (*i.e.* L1 and L2). Therefore, for the last two weeks of measurements, we propose implementing an equivalent circuit that takes into account the individual contributions of layers L1 and L2 to R_c. Figure 13D shows the proposed equivalent circuit (ECC). In the ECC, R_{sol}, Q_{dl} and R_{ct} represent solution resistance, double layer capacitance and charge transfer resistance, respectively. $R_{c1(TiN-L1)}$ (L1 resistance) and $Q_{c1(TiN-L1)}$ (L1 capacitance) represent the individual contribution of layer L1 and $R_{c2(TiN-L2)}$ and $Q_{c2(TiN-L2)}$ represent the individual contribution of layer L2. Therefore, the R_c for weeks 6 and 7, as shown in Figure 12A, are the sum of the contributions from layers L1 and L2 ($R_c = R_{c1(TiN-L1)} + R_{c2(TiN-L2)}$), as detailed in Figure 12B.

The results indicate that L1 contributed more than L2 over the last few weeks. In fact, in week 7, $R_{c2(TiN-L2)}$ has a very low value compared to $R_{c1(TiN-L1)}$, indicating that layer L2 has decreased its level of protection. This allows ions to flow more easily towards the L1-L2 interface, probably causing the accumulation of electrolyte solution at this interface and undoubtedly promoting electrochemical activity in the substrate-coating interface. This could be the main reason why the EIS technique can discern the individual contributions of the two layers. To verify the low-frequency behaviour of the TiN-bilayer, impedance measurements were extended over two weeks (weeks 8 and 9). The Nyquist and Bode plots for weeks 8 and 9 exhibited low-frequency characteristics similar to those observed in the curves for weeks 6 and 7 (see Figures 13A *to 13*C), prompting the application of ECC. The results R_{ct}, R_c and R_p obtained from the impedance data fitted by the ECC implementation for weeks 8 and 9 are shown in Figure 12A, and in more details in Figure 12B. These figures indicate the degree of degradation of layer L2. Figure 12B shows the general contribution of layers L1 and L2 ($R_{c1(TiN-L1)}$ and $R_{c2(TiN-L2)}$, respectively) over weeks 6, 7, 8 and 9. Overall, the contribution of layer L2 is small relative to that of layer L1 over the last four weeks. This behaviour suggests that the L2 layer is heavily infiltrated by the electrolyte solution and therefore does not represent an effective barrier against the aggressive medium during these final weeks. Therefore, over time, layer L1 becomes the only effective barrier against ion diffusion towards the substrate surface. However, it also slowly becomes infiltrated by the electrolyte solution over time, resulting in the TiN-bilayer coating system losing its protective capacity. Additionally, R_{ct} tends to decrease during the last two weeks, indicating that electrochemical activity on the substrate surface increases over time. In fact, R_{ct} decreases even though when $R_{c1(TiN-L1)}$ increases during weeks 8 and 9. This behaviour may be due to the fact that these increases in $R_{c1(TiN-L1)}$ are insufficient to mitigate corrosion at the substrate surface. This may be because these increases in $R_{c1(TiN-L1)}$ are certainly due to the blocking of some pathways in the L1 layer; however, these blocked pathways may represent a small proportion of the total, and therefore, the corrosion process cannot be mitigated, and it will continue on the substrate surface.

From this point of view, it is important to note that, although R_p is a parameter that indicates the level of insulation that the coating system offers to the substrate, R_{ct} is equally important and can sometimes behave in a way that contrasts with R_c and R_p. This is mainly because R_{ct} is the result of the interaction between the substrate surface and electrolyte solution (an aggressive medium) that arrives from the coating surface through pathways and accumulates at the substrate-coating interface.

Therefore, although this interaction is fuelled by the arrival and activity of aggressive ions, it will be difficult to mitigate corrosion on the substrate surface, even if some pathways are obstructed, thereby increasing the R_c parameter. Consequently, for coatings highly susceptible to defects, which can act as ion diffusion pathways (such as the TiN coating in our case), analysis of R_p alone may not be sufficient to determine the electrochemical behaviour over time, because the R_p could hide what is actually occurring at the substrate-coating interface. Therefore, it is very important for the analysis of R_{ct} and R_c to better understand the electrochemical response of the coating system under aggressive environmental conditions.

From the over-time analysis of the TiN-bilayer coating system, it can be concluded that, for some coating systems, as immersion time increases, the relationship between R_{ct} and R_c becomes more complex. For example, increases in R_c from the result of pathways clogging should produce increases in R_{ct}, *i.e.* a decrease in electrochemical activity at the substrate-coating interface. However, as immersion time passes, these increases in R_c do not seem to be sufficient to mitigate the corrosion process at the substrate-coating interface, where R_{ct} can remain constant. In other cases, the R_{ct} can decrease despite an increase in R_c, indicating that the electrochemical activity has reached a level at which clogging a few pathways in the coating system cannot mitigate the corrosion process at the substrate-coating interface. This situation indicates the level of deterioration of the coating system. The resistance values for weeks 8 and 9 shown in Figure 12B illustrate this behaviour, where R_c for each layer ($R_{c1(TiN\text{-}L1)}$ and $R_{c2(TiN\text{-}L2)}$) increase compared to the same values in the week 8, *i.e.* R_c(sum of $R_{c1(TiN\text{-}L1)}$ and $R_{c2(TiN\text{-}L2)}$) increase from 29.192 (week 8) to 33.644 kΩcm^2, this increase in R_c indicate an increase in the insulation capacity of the coating system, which should decrease the electrochemical activity in the substrate-coating interface increasing the R_{ct}, but this does not occur, the R_{ct} decrease from 23.191 (week 8) to 15.720 kΩcm^2 indicating that the electrochemical activity increase. Therefore, this result suggests that in the last weeks of immersion, the substrate-coating interface is very active and although the coating system undergoes clogging of some pathways, increasing the R_c, this cannot mitigate the corrosion process in the substrate surface, which indicates the lost protective capacity of the TiN-bilayer coating.

Figure 14 shows how R_{ct}, R_c and R_p vary over time for the W/TiN-bilayer coating system. It shows that the W/TiN-bilayer coating system exhibits better behaviour in an aggressive medium than the TiN-bilayer coating system. Although the coating system showed some instability during immersion (with the R_p decreasing and increasing), the R_{ct} remained above 100 kΩcm^2, indicating good performance compared to the TiN-bilayer coating system.

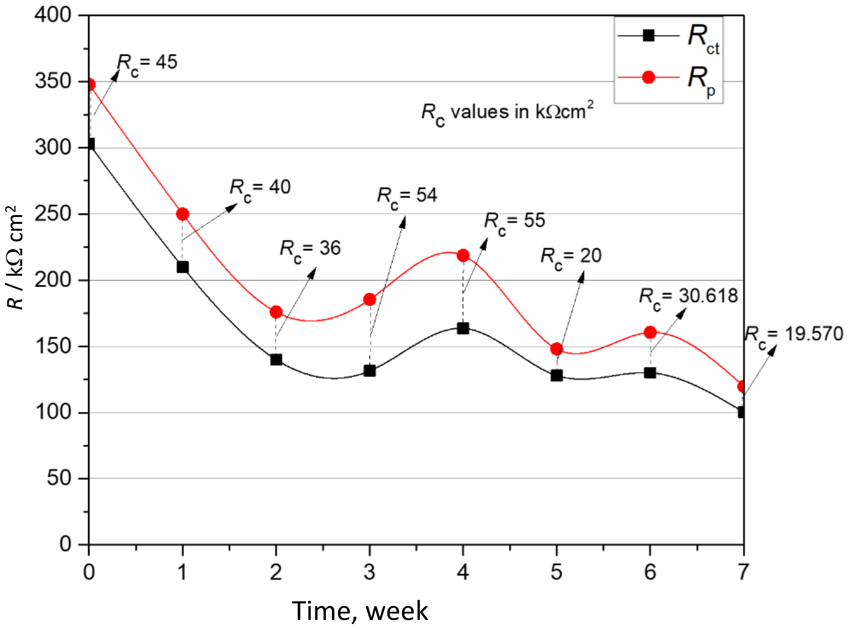

Figure 14. *Time changes of EIS generated R_{ct}, R_c and R_p values for W/TiN-bilayer coating*

However, it is important to point out that among weeks 5 and 6, the R_c increases to about 10 kΩ cm²; however, the values in R_{ct} differ by barely 2 kΩ cm² (as shown in Figure 14), indicating that at the substrate-coating interface, the electrochemical activity becomes important. Nevertheless, and as discussed in previous paragraphs, the W film on the TiN-bilayer system can be considered a diffusion barrier that delays the deterioration of the TiN layers involved in the coating system. The W film's favourable behaviour is partly due to the natural properties of the W element. In our particular case, however, the diffusion process between the W film and L2 (already discussed above with structural characteristics of obtained coating systems) suggests that the W thin film is essentially composed of two parts (see Figure 6B): the first part contains only α-W, and immediately below it, the second part contains a W-TiN compound related to the W-Ti-N ternary alloy. Therefore, when a W-Ti-N ternary alloy is part of a W/TiN-bilayer coating, it significantly contributes to the high corrosion resistance of the W thin film because the W-Ti-N systems are used as diffusion barriers due to their anticorrosive properties [20].

Mechanical properties

Hardness

The mechanical properties of the coatings were determined by nanoindentation tests using indentation loads in the μN range. Figure 15A illustrates the load-unload curves and Figure 15B shows the indentation stress (σ_i) *vs.* contact depth (h_c) curves, which can be used to define the mechanical properties of different materials. The σ_i vs. h_c curves were obtained considering the stiffness parameter *S* (d*P*/d*h*) for each indentation test, where *P* and *h* are the applied load and the indentation depth.

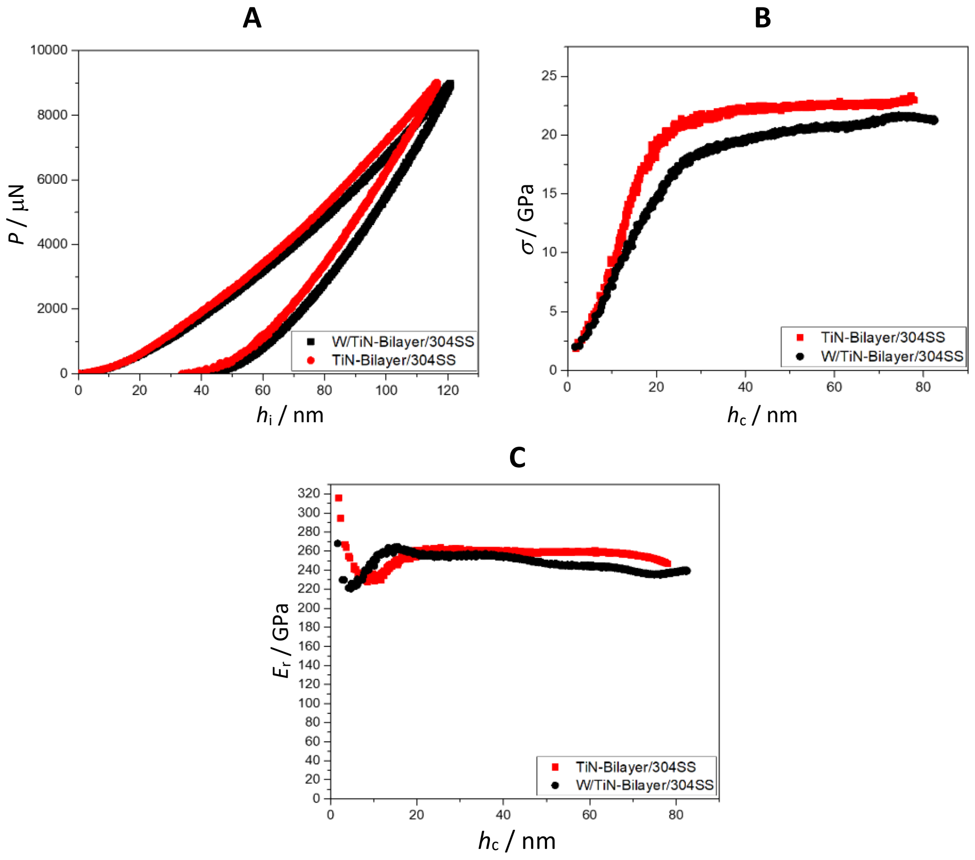

Figure 15. *A) Load-unload curves for* both *coating systems, B)* σ_i vs. h_c *for both coating systems, C) reduced composite elastic modulus* vs. h_c *for both systems*

The experimental values of the *S* parameter were described as a function of the indentation load by a polynomial function. We used this method in previous work [40]. The contact depth (h_c) is calculated using Equation (2) [41]:

$$h_c = h_i \text{-} 0.75\frac{P}{S} \tag{2}$$

where *P* is the applied load and h_i is the indentation depth.

Comparing the load-unload curves, it can be observed that the W/TiN-bilayer has lower mechanical properties than the TiN-bilayer coating system. The load-unload curve for the W/TiN-bilayer coating has a slight shift to the right compared to the load-unload curve for TiN-bilayer coating, indicating that the maximum penetration depth of the W/TiN-bilayer is greater than that of the TiN-bilayer. Thus, this behaviour suggests a slight decrease in the mechanical properties of the W/TiN-bilayer coating system compared to the TiN-bilayer coating system. This feature is reflected in the σ_i *vs.* h_c curves calculated from load-unload curve data (Figure 15B). In this graph, the curve corresponding to the W/TiN-bilayer coating is below the curve corresponding to the TiN-bilayer coating curve. Therefore, from these results, the hardness for the W/TiN-bilayer and TiN-bilayer coatings is approximately 21.2 and 22.9 GPa, respectively. This difference in hardness between the two systems is undoubtedly due to the W thin film having a lower intrinsic hardness than the TiN layer. To obtain information about the influence of the mechanical properties of the W thin film on the global system, the JH model has been used. This model was proposed by Jonsson *et al.* [42]. Thus, the composite hardness is expressed by Equation (3):

$$H_\mathrm{c} = \frac{A_\mathrm{f}}{A} H_\mathrm{f} + \frac{A_\mathrm{s}}{A} H_\mathrm{s} \tag{3}$$

where H_f and H_s are the hardness of the film and the substrate and A_f/A and A_s/A are the area fraction corresponding to the coating and the substrate, based on the projected area that the indenter produces when it penetrates from the surface of the coating. For practical purposes, the L2 layer (TiN coating) is considered the substrate for the W thin film, since the maximum contact depth is only about 80 nm. In fact, the load levels used in this work yield a penetration depth that is much less than 10 % of the thickness of the coating system, resulting in a very small influence of the L1 layer and the 304SS substrate on the mechanical properties of the W thin film. Thus, the hardness values obtained from the application of the model are approximately 18 and 24 GPa for W thin film and the L2 layer, respectively.

Elastic modulus

In the same sense to the hardness, the reduced composite elastic modulus (E_r) *vs.* contact depth (h_c) for both systems was calculated from load-unload curves (Figure 15C) using equation (4)[14]:

$$S = \frac{\mathrm{d}P}{\mathrm{d}h} = \frac{2\beta}{\pi^{1/2}} E_\mathrm{r} A_\mathrm{c}^{1/2} \tag{4}$$

From Equation (4) it is possible to rewrite the reduced composite elastic modulus, Equation (5)

$$E_\mathrm{r} = \frac{S\sqrt{\pi}}{2\beta\sqrt{A_\mathrm{c}}} \tag{5}$$

where A_c is the contact area projected by the indenter, calculated as a function of h_c, and expressed by Equation (6):

$$Ah_\mathrm{c} = C_0 h_\mathrm{c}^2 + C_1 h_\mathrm{c} + C_2 h_\mathrm{c}^{1/2} + C_3 h_\mathrm{c}^{1/4} + C_4 h_\mathrm{c}^{1/8} + C_5 h_\mathrm{c}^{1/16} \tag{6}$$

The form of this expression was developed by Oliver and Pharr [41,43], where C_0……C_5 are constants determined by calibrating the nanoindentation test using a homogeneous material such as fused quartz. $\beta \approx 1.05$ is a correction factor that accounts for stiffness deviations due to the lack of axial symmetry of the pyramidal indenter. Therefore, from these results, the hardness for the W/TiN-Bilayer and TiN-Bilayer coatings is approximately 254 and 263 GPa, respectively. Equal to the hardness, the reduced elastic modulus for the W film E_rf was also calculated using the JH model to determine the individual value of this property for the W thin film, taking into account the considerations that comment Puchi-Cabrera *et al.* [44] for this calculus. The obtained values for E_{rf} (W thin film) and E_{rs} (TiN coating) are 205 and 258 GPa, respectively.

Mechanical properties relationship

The mechanical properties of both composite coating systems are summarized in Table 2.

***Table 2**. Mechanical properties for both coating systems.*

Composite coating systems	Hardness, GPa	Reduced composite elastic modulus, GPa
W/TiN-bilayer	21.2	254
TiN-bilayer	22.9	262

As shown in Table 2, the results suggest that the two coating systems exhibit very similar mechanical behaviour. The hardness difference between the two systems is just 1.7 GPa, and the elastic modulus difference is only 10 GPa. This indicates that the two systems exhibit similar mechanical properties. As mentioned in previous paragraphs, the W thin film exhibits a value of 18 GPa, and therefore, its contribution tends to slightly decrease the overall hardness of the W/TiN-bilayer compared with the TiN-Bilayer system. However, it is notable that the hardness of the W thin film is very high, despite being grown in a vacuum chamber at a pure argon working pressure and despite its low thickness. Regarding the diffusion process between the L2 layer and the W thin film, as discussed in previous sections, we believe that the hardness of the W thin film is actually a combination of the two parts (see Figure 6B), where the first part is pure W and the second part is a W-TiN compound formed during the interlayer diffusion process. This compound can improve the film's mechanical properties through direct interaction with TiN and its thin thickness, making the second part's contribution significant. Therefore, a high hardness value (18 GPa) could be expected from the W thin film. This behaviour demonstrates a strong relationship between the substrate's nature and the film's mechanical properties. Therefore, it is important to note that the diffusion process in multilayer coating systems (which can occur during or after film growth) is critical because it can form new interfaces that ultimately determine the properties of the coating system and improve its performance. Based on the above, the W/TiN Bilayer system produced under the experimental parameters specified in this study can be considered an alternative hard-diffusion barrier.

Conclusions

The present work has shown that a W thin film deposited on a TiN bilayer coating exhibits a cubic α-W phase along the [110] direction. In the case of TiN coating, the preferential directions were the [111] and [200], however, peaks of lower intensity appear, indicating the directions [220], [311] and [222]. AES results show a diffusion zone defining a W-TiN composite that acts as an interface between the W thin film and the L2 layer. Magnetron sputtered TiN layers L1 and L2 grown at substrate temperature of 250 °C, show pyramidal grain structures. Particular rose-shaped nodular defects were also found in the L1 (TiN/304SS) layer. Regarding the electrochemical behaviour, the high R_{ct} and R_{p} over time for the W/TiN-bilayer coating system compared to the TiN-bilayer coating system showed that the W thin film deposited on the TiN-bilayer acts as a barrier, increasing the corrosion resistance. It is also important to point out that for TiN-bilayer coating system at the end of the immersion time (the last three weeks) the R_{c} tends to increase, however the R_{ct} tends to decrease, indicating the deterioration level of the coating system, besides, the results for the last three weeks also showed a small individual contribution of the L2 layer to R_{c} compared to the contribution of the L1 layer, another indication of damage of the TiN-bilayer coating system. Therefore, the results suggest that, as time passes, the relationship between R_{ct} and R_{c} becomes complex, because although R_{c} increases, R_{ct} may tend to decrease, indicating strong electrochemical activity in the substrate-coating interface and, hence, the loss of the insulation capacity of the coating system. In addition, this study demonstrates that the electrochemical behaviour of both coating systems obtained from the initial measurements is generally consistent with that observed over time. Specifically, the corrosion performance of the W/TiN bilayer coating system is superior to that of the TiN bilayer coating system. It should be noted that certain characteristics can only be determined over time, as is the case with the TiN-bilayer coating system.

Comparing the mechanical properties of the coating systems, it can be concluded that the W/TiN-bilayer coating system has a lower composite hardness than the TiN-bilayer coating system, but this difference in hardness is small (about 1.7 GPa). The results suggest that this difference is mainly due to the W thin film deposited on the TiN coating (layer L2), which has lower mechanical properties than the TiN substrate, which has an obvious effect on the global mechanical properties of the coating system. However, the individual hardness of the W film is high (18 GPa) and it can be considered as a hard thin film. The results suggest that the diffusion process at the interface (layer L2-W thin film) may have an important contribution to the final definition of the properties of the W thin film. Considering the differences in the mechanical properties of both coating systems, which are relatively small, as well as considering the electrochemical behaviour, which indicates a substantial improvement with the incorporation of the W thin film, the W/TiN-bilayer coating system can be an alternative as a hard and anticorrosive coating, incorporating the knowledge of the other properties associated with W compounds.

Conflicts of Interest: *The authors declare no conflicts of interest.*

Acknowledgements: *The authors would like to thank E. Flores Aquino, J. Davalos, G. Garcia (r.i.p) from CICESE, and M. Sainz, J. Peralta, P. Casillas, I. Gradillas, J. Mendoza and E. Aparicio of CNyN-UNAM for their collaboration. The Authors also would like to thank to Dra. Yeni Sanchez, Mr. Freddy Jimenez of Centro de Física- IVIC and Dr. Sergio Serna Barquera (r.i.p) of CIICap-UAEM, as well as to Mr. I. Puente-Lee of Facultad de Química-UNAM, Mr. H. Hinojosa and Mr. A. Gonzalez (r.i.p.) of ICF-UNAM for their technical support*

Funding: *This research was supported by FONACIT project Nº 2022OPGP39.*

References

[1] L. Maillé, C. Sant, P. Garnier, A nanometer scale surface morphology study of W thin films, *Materials Science and Engineering C* **23** (2003) 913-918. https://dx.doi.org/10.1016/j.msec.2003.09.114

[2] A. H. Macias, D. C. Kothari, V. S. Kalyana, M. Subramanian, G. K. Dey, S. K. Gupta, Mechanical characterization of thin amorphous tungsten-carbon (W_xC_y) films prepared by DC-cosputtering, *Vacuum* **77** (2005) 173-176. https://dx.doi.org/10.1016/j.vacuum.2004.07.006

[3] J. Yu, W. Han, Z. Chen, K. Zhu, Blistering of tungsten films deposited by magnetron sputtering after helium irradiation, *Fusion Engineering and Design* **129** (2018) 230-235. https://dx.doi.org/10.1016/j.fusengdes.2018.02.091

[4] A. M. Engwall, S. J. Shin, J. Bae, Y. M. Wang, Enhanced properties of tungsten films by high-power impulse magnetron sputtering, *Surface and Coatings Technology* **363** (2019) 191-197. https://dx.doi.org/10.1016/j.surfcoat.2019.02.055

[5] I. Djerdj, A. M. Tonejc, A. Tonejc, N. Radić, XRD line profile analysis of tungsten thin films, *Vacuum* **80** (2005) 151-158. https://dx.doi.org/10.1016/j.vacuum.2005.08.017

[6] W. Meng, L. Wei, Z. Jingwen, The Characterization of Superconducting Tungsten Thin Films Deposited by DC Magnetron Sputtering, *3rd International Conference on Integrated Circuits and Microsystems*, IEEE, 2018, 24-26 November 2018, Shangai, China, pp. 268-272. https://dx.doi.org/10.1109/ICAM.2018.8596502

[7] S. Fritze, M. Chen, L. Riekehr, B. Osinger, M. A. Sortica, A. Srinath, A. S. Menon, E. Lewin, D. Primetzhofer, J. M. Wheeler, U. Jansson, Magnetron sputtering of carbon supersaturated tungsten films - A chemical approach to increase strength, *Materials and Design* **208** (2021) 109874. https://dx.doi.org/10.1016/j.matdes.2021.109874

[8] S. Camelio, T. Girardeau, L. Pichon, A. Straboni, C. Fayoux, P. Gú, Transformation of the semi-transparent into the metallic phase of zirconium nitride compounds by implantation at controlled temperature: the evolution of the optical properties, *Journal of Optics A* **2** (2000) 442-447. http://iopscience.iop.org/1464-4258/2/5/315

[9] J. Zuo, Y. Xie, J. Zhang, Q. Wei, B. Zhou, J. Luo, Y. Wang, Z. M. Yu, Z. G. Tang, TiN coated stainless steel bracket: Tribological, corrosion resistance, biocompatibility and mechanical performance, *Surface and Coatings Technology* **277** (2015) 227-233. https://dx.doi.org/10.1016/j.surfcoat.2015.07.009

[10] C. J. Yang, F. H. Lu, Shape and size control of Cu nanoparticles by tailoring the surface morphologies of TiN-coated electrodes for biosensing applications, *Langmuir* **29** (2013) 16025-16033. https://dx.doi.org/10.1021/la403719c

[11] P. Yi, L. Zhu, C. Dong, K. Xiao, Corrosion and interfacial contact resistance of 316L stainless steel coated with magnetron sputtered ZrN and TiN in the simulated cathodic environment of a proton-exchange membrane fuel cell, *Surface and Coatings Technology* **363** (2019) 198-202. https://dx.doi.org/10.1016/j.surfcoat.2019.02.027

[12] K. Sarkar, P. Jaipan, J. Choi, T. Haywood, D. Tran, N. R. Mucha, S. Yarmolenko, O. Scott-Emuakpor, M. Sundaresan, R. K. Gupta, D. Kumar, Enhancement in corrosion resistance and vibration damping performance in titanium by titanium nitride coating, *SN Applied Sciences* **2** (2020) 893. https://dx.doi.org/10.1007/s42452-020-2777-1

[13] D. Turcio-Ortega, S. E. Rodil, S. Muhl, Electrochemical Behavior of Titanium Thin Films Obtained by Magnetron Sputtering, *Materials Science* **14** (2008) 15-19.

[14] B. Subramanian, M. Jayachandran, Electrochemical corrosion behavior of magnetron sputtered TiN coated steel in simulated bodily fluid and its hemocompatibility, *Materials Letters* **62** (2008) 1727-1730. https://dx.doi.org/10.1016/j.matlet.2007.09.072

[15] S. H. Yao, Y. L. Su, W. H. Kao, K. W. Cheng, A wear-resistant coating-oxidized graded multilayer TiN/W coating, *Materials Letters* **64** (2010) 99-101. https://dx.doi.org/10.1016/j.matlet.2009.10.026

[16] H. L. Sun, Z. X. Song, D. G. Guo, F. Ma, K. W. Xu, Microstructure and mechanical properties of nanocrystalline tungsten thin films, *Journal of Materials Science & Technology* **26** (2010) 87-92. https://dx.doi.org/10.1016/S1005-0302(10)60014-X

[17] A. E. Lita, D. Rosenberg, S. Nam, A. J. Miller, R. E. Schwall, R. Mirin, Tuning of tungsten thin film superconducting transition temperature for fabrication of photon number resolving detectors, *IEEE Transactions on Applied Superconductivity* **15** (2005) 3528-3531. https://dx.doi.org/10.1109/TASC.2005.849033

[18] A. U. Chaudhry, B. Mansoor, T. Mungole, G. Ayoub, D. P. Field, Corrosion mechanism in PVD deposited nano-scale titanium nitride thin film with intercalated titanium for protecting the surface of silicon, *Electrochimica Acta* **264** (2018) 69-82. https://dx.doi.org/10.1016/j.electacta.2018.01.042

[19] A. Fragiel, R. Machorro, J. Muñoz-Saldaña, J. Salinas, L. Cota, Correlation between optical characterization of the plasma in reactive magnetron sputtering deposition of Zr-N on SS

316L and surface and mechanical properties of the deposited films, *Applied Surface Science* **254** (2008) 4632-4637. https://dx.doi.org/10.1016/j.apsusc.2008.01.104

[20] W. Qingxiang, L. Shuhua, W. Xianhui, F. Zhikang, Diffusion barrier performance of amorphous WTiN films in Cu metallization, *Vacuum* **84** (2010) 1270-1274. https://dx.doi.org/10.1016/j.vacuum.2010.02.002

[21] A. V. Kuchuk, V. P. Kladko, O. S. Lytvyn, A. Piotrowska, R. A. Minikayev, R. Ratajczak, Relationship between condition of deposition and properties of W-Ti-N thin films prepared by reactive magnetron sputtering, *Advanced Engineering Materials* **8** (2006) 209-212. https://dx.doi.org/10.1002/adem.200500263

[22] J. S. Colligon, *Physical Vapor Deposition*, in *Non-equilibrium Processing of Materials*, C. Suryanarayana, Ed., Elsevier, 1996, 225-253. https://doi.org/10.1016/S1470-1804(99)80055-8

[23] X. Qi, H. He, P. Hu, S. Bai, Z. Jiang, Y. Zhao, M. Li, F. Wan, L. Zhang, Y. Zhou, S. Chen, F. Ren, Pyramidal structure that promotes the photothermal effects of TiN films for de-icing applications, *Ceramics International* **51** (2025) 27770-27781. https://dx.doi.org/10.1016/j.ceramint.2025.03.020

[24] V. Chawla, R. Jayaganthan, R. Chandra, Structural characterizations of magnetron sputtered nanocrystalline TiN thin films, *Materials Characterization* **59** (2008) 1015-1020. https://dx.doi.org/10.1016/j.matchar.2007.08.017

[25] P. Panjan, D. Kek Merl, F. Zupanič, M. Čekada, M. Panjan, SEM study of defects in PVD hard coatings using focused ion beam milling, *Surface and Coatings Technology* **202** (2008) 2302-2305. https://dx.doi.org/10.1016/j.surfcoat.2007.09.033

[26] J. Vetter, M. Stuber, S. Ulrich, Growth effects in carbon coatings deposited by magnetron sputtering, *Surface and Coatings Technology* **174-175** (2003) 553-558. https://dx.doi.org/10.1016/S0257-8972(03)00585-2

[27] S. Calderon, C. F. A. Alves, N. K. Manninen, A. Cavaleiro, S. Carvalho, Electrochemical corrosion of nano-structured magnetron-sputtered coatings, *Coatings* **9** (2019) 682. https://dx.doi.org/10.3390/coatings9100682

[28] R. N. Tait, T. Smy, S. K. Dew, M. J. Brett, Nodular Defect Growth and Structure in Vapor Deposited Films, *Journal of Vacuum Science & Technology B: Microelectronics and Nanometer Structures* **13** (1995) 2345-2353. https://dx.doi.org/10.1116/1.588077

[29] P. Panjan, A. Drnovšek, P. Gselman, M. Čekada, M. Panjan, Review of growth defects in thin films prepared by PVD techniques, *Coatings* **10** (2020) 447. https://dx.doi.org/10.3390/COATINGS10050447

[30] B. Abdallah, M. Kakhia, W. Alsadat, Deposition of TiN and TiAlVN thin films by DC magnetron sputtering: Composition, corrosion and mechanical study, *International Journal of Structural Integrity* **11** (2020) 819-831. https://dx.doi.org/10.1108/IJSI-10-2019-0105

[31] K. Taweesup, P. Visuttipitukul, N. Yongvanich, G. Lothongkum, Corrosion behavior of Ti-Cr-N coatings on tool steel substrates prepared using DC magnetron sputtering at low growth temperatures, *Surface and Coatings Technology* **358** (2019) 732-740. https://dx.doi.org/10.1016/j.surfcoat.2018.11.082

[32] A. González-Hernández, A. B. Morales-Cepeda, M. Flores, J. C. Caicedo, W. Aperador, C. Amaya, Electrochemical properties of TiWN/TiWC multilayer coatings deposited by RF-magnetron sputtering on AISI 1060, *Coatings* **11** (2021) 797. https://dx.doi.org/10.3390/coatings11070797

[33] R. M. Fonseca, R. B. Soares, R. G. Carvalho, E. K. Tentardini, V. F. C. Lins, M. M. R. Castro, Corrosion behavior of magnetron sputtered NbN and $Nb_{1-x}Al_xN$ coatings on AISI 316L stainless steel, *Surface and Coatings Technology* **378** (2019) 124987. https://dx.doi.org/10.1016/j.surfcoat.2019.124987

[34] X. Yu, J. Wang, L. Wang, W. Huang, Fabrication and characterization of CrNbSiTiZr high-entropy alloy films by radio-frequency magnetron sputtering via tuning substrate bias, *Surface and Coatings Technology* **412** (2021) 127074. https://dx.doi.org/10.1016/j.surfcoat.2021.127074

[35] A. Dettlaff, L. Koltunowicz, M. Szczepanik, A. Gilewicz, P. Zawadzki, P. M. Nuckowski, B. Warcholiński, Highly Oriented Zirconium Nitride and Oxynitride Coatings Deposited via High-Power Impulse Magnetron Sputtering: Crystal-Facet-Driven Corrosion Behavior in Domestic Wastewater, *Advanced Engineering Materials* **23** (2021) 2001349. https://dx.doi.org/10.1002/adem.202001349

[36] C. Ramoul, N. E. Beliardouh, R. Bahi, C. Nouveau, A. Djahoudi, M. J. Walock, Surface performances of PVD ZrN coatings in biological environments, *Tribology - Materials, Surfaces and Interfaces* **13** (2019) 12-19. https://dx.doi.org/10.1080/17515831.2018.1553820

[37] A. Olayinka, A. Esther, O. Philip, Examination of electrochemical corrosion properties of titanium carbide thin film grown by RF magnetron sputtering, *Materials Today: Proceedings* **44** (2021) 994-999. https://dx.doi.org/10.1016/j.matpr.2020.11.170

[38] V. Vivier, M. E. Orazem, Impedance Analysis of Electrochemical Systems, *Chemical Reviews* **122** (2022) 11131-11168. https://dx.doi.org/10.1021/acs.chemrev.1c00876

[39] J. Vega, H. Scheerer, G. Andersohn, M. Oechsner, Experimental studies of the effect of Ti interlayers on the corrosion resistance of TiN PVD coatings by using electrochemical methods, *Corrosion Science* **133** (2018) 240-250. https://dx.doi.org/10.1016/j.corsci.2018.01.010

[40] A. Fragiel, M. H. Staia, J. Muñoz-Saldaña, E. S. Puchi-Cabrera, C. Cortes-Escobedo, L. Cota, Influence of the N_2 partial pressure on the mechanical properties and tribological behavior of zirconium nitride deposited by reactive magnetron sputtering, *Surface and Coatings Technology* **202** (2008) 3653-3660. https://dx.doi.org/10.1016/j.surfcoat.2008.01.001

[41] W. C. Oliver, G. M. Pharr, An improved technique for determining hardness and elastic modulus using load and displacement sensing indentation experiments, *Journal of Materials Research* **7** (1992) 1564-1583. https://dx.doi.org/10.1557/jmr.1992.1564

[42] B. Jonsson, S. Hogmark, Hardness measurements of thin films, *Thin Solid Films* **114** (1984) 257-269. https://dx.doi.org/10.1016/0040-6090(84)90123-0

[43] W. C. Oliver, G. M. Pharr, Measurement of hardness and elastic modulus by instrumented indentation: Advances in understanding and refinements to methodology, *Journal of Materials Research* **19** (2004) 3-20. https://doi.org/10.1557/jmr.2004.19.1.3

[44] E. S. Puchi-Cabrera, M. H. Staia, A. Iost, *A description of the composite elastic modulus of multilayer coated systems*, *Thin Solid Films* **583** (2015) 177-193. https://dx.doi.org/10.1016/j.tsf.2015.02.078

©2026 by the authors; licensee IAPC, Zagreb, Croatia. This article is an open-access article distributed under the terms and conditions of the Creative Commons Attribution license (http://creativecommons.org/licenses/by/4.0/)